Available online at www.sciencedirect.com
SCIENCE DIRECT®
Journal of Sound and Vibration 274 (2004) 761–776
JOURNAL OF SOUND AND VIBRATION
www.elsevier.com/locate/jsvi

Power spectral density analysis for damage identification and location

S. Liberatore, G.P. Carman*

Mechanical and Aerospace Engineering Department, School of Engineering, University of California, Engineering IV, 420 Westwood Plaza, Los Angeles, CA 90095, USA

Received 9 July 2002; accepted 13 June 2003

Abstract

A method for both identification and localization of structural damage is proposed and implemented on a simply supported beam. The results are predicted with an analytical model and verified with an experimental test set-up consisting of an aluminum beam with one actuator and one sensor, both piezoelectrics. The method estimates the energy localized in bandwidth regions near resonance that are the most sensitive to damage. The energy is estimated by power spectral density analysis and quantified by means of its root mean square value. These values are combined with mode shapes to locate damage. The method is evaluated with small masses used to simulate damage and or small cuts to simulate damage and good agreement is obtained between experiments and analysis.

1. Introduction

Structural damage detection can considerably increase safety and reduce maintenance costs. The goal for damage detection is to identify damage at the earliest stage of development. Numerous methods have been proposed and among them, dynamic response based approaches are prominent. However, to date these methods have relatively poor sensitivity.

Cawley and Adams [1] were one of the first who published works that used frequency shifts to detect damage. A more recent example of a similar approach can be found in Armon et al. [2], in which the frequency shifts of a cantilever beam were ordered in a crescent numerical succession and their indexes (ranks) were used to estimate the damage location. Narkis [5] proposed a closed form solution of the damage localization problem using shifts in the first two natural frequencies

*Corresponding author. Tel.: +1-310-825-6030; fax: +1-310-206-2302.
E-mail address: carman@seas.ucla.edu (G.P. Carman).

0022-460X/$ - see front matter © 2003 Elsevier Ltd. All rights reserved.
doi:10.1016/S0022-460X(03)00785-5

for a simply supported beam under longitudinal and bending vibrations. Recently, Morassi [6] extended the work of Narkis to include axially vibrating rods under generic boundary conditions. Morassi showed that the problem is generally ill-posed because two cracks at different locations produce similar changes in a pair of natural frequencies. However, in Ref. [6] it was shown that a careful choice of the data could significantly reduce the ill conditioning of the diagnostic problem. Morassi and Dilena [7] proposed a method that was able to detect a point mass in a beam and also estimated the mass size. However, their method requires very accurate measurements and an analytical solution that is not always available. Farrar et al. [8] used frequency shifts to identify damage in a highway bridge and showed that the method was not sufficiently sensitive to detect damage. In general, natural frequencies shift by only a few percent and therefore are relatively insensitive to damage.

Mode shapes can also be used to identify and localize damage. A modal assurance criterion (MAC) introduced by West [9] and its modified version (COMAC), introduced by Kim et al. [10], along with numerous variations [3], have been proposed and tested in laboratory demonstrations. However, Pandey et al. [11] showed that MAC and COMAC techniques were insensitive to damage location for a cantilever and a simply supported beam. Pandey proposed monitoring mode shape curvature changes to increase sensitivity with respect to MAC and COMAC techniques. Although this approach detected and localized damage, it relied on numerical schemes that produce relatively large errors when compared with other changes.

Strain energy methods have also been proposed to detect damage. A damage index [12], defined by the ratio of strain energy between damaged and undamaged states, was used to detect damage. Recently, Park et al. [13] used an FEM model to analyze a damage index and compared the results with visual inspection of a I-40 highway damaged bridge. While moderately successful, many predictions were not verified by inspection. These and other methods based on a damage index parameter have been proposed as diagnostic tools with details that can be found in two extensive reviews [3,4].

The method analytically and experimentally studied in this paper utilizes both frequency shifts and mode shape changes to infer damage and location. Dynamic structural response is obtained from piezoelectric point actuators and sensors placed on a simply supported beam. Narrow bandwidths near resonant frequencies are chosen to maximize sensitivity. By using a Power Spectral Density (PSD) analysis, the energy associated with the narrow bandwidths is evaluated and then quantified by means of a Root Mean Square (RMS) value. The RMS obtained from the undamaged structure is compared with the RMS of the damaged one. This process appears to increase the sensitivity when compared with other methods reviewed in this paper. The RMS changes are used to define a DLM index that can infer damage in the structure. This index is however unable to localize the damage position. For this purpose, the RMS values are utilized in combination with structural mode shapes to define a damage location function, $DL(x)$, that locates both a point mass and a saw cut in the structure.

2. Analytical model

A simply supported beam is modelled with both bending and axial deformation. The governing dynamic equations for the structure are obtained from an energetic formulation of the problem

[14]. The beam's kinetic and potential energy are expressed in terms of displacements

$$K = \frac{1}{2}\rho \int_V \left\{ \left(\frac{\partial U(x,z,t)}{\partial t}\right)^2 + \left(\frac{\partial W(x,z,t)}{\partial t}\right)^2 \right\} \mathrm{d}V, \quad P = \frac{1}{2}\int_V E\left(\frac{\partial U(x,z,t)}{\partial x}\right)^2 \mathrm{d}V, \tag{1}$$

where $U(x,z,t)$ and $W(x,z,t)$ are longitudinal and transversal displacements respectively while ρ and E are the volume density and Young's modulus of the structure.

The generalized Hamilton principle for a piezoelectric requires substituting the potential energy with the electric enthalpy to include electroelastic coupled phenomenon [15]. The enthalpy can be written as

$$H_a = \frac{1}{2}\int_{V_a} \left\{ \bar{E}_a^E \left(\frac{\partial U}{\partial x}\right)^2 - 2d_{31}\bar{E}_a^E \frac{\Delta\varphi_a}{t_a}\left(\frac{\partial U}{\partial x}\right) - \epsilon_{33}^{\varepsilon}\left(\frac{\Delta\varphi_a}{t_a}\right)^2 \right\} \mathrm{d}V_a \tag{2}$$

while the kinetic energy is

$$K_a = \frac{1}{2}\rho_a \int_{V_a} \left\{ \left(\frac{\partial U(x,z,t)}{\partial t}\right)^2 + \left(\frac{\partial W(x,z,t)}{\partial t}\right)^2 \right\} \mathrm{d}V_a. \tag{3}$$

In Eqs. (2) and (3), ρ_a and $\bar{E}_a^E$ are the volume density and Young's modulus of the actuator at constant electric field, d_{31} is piezoelectric stress/charge coefficient, $\Delta\varphi_a$ is the applied voltage, $\epsilon_{33}^{\varepsilon}$ is the piezoelectric material permittivity at constant strain and t_a is the actuator thickness.

Eq. (2) could be used for defining the potential energy of the sensor as well. However, for the sensor, the strain energy contribution to the enthalpy is much greater than the remaining electrical and electromechanical terms that can be neglected. With these assumptions, the potential energy for the sensor can be written as

$$P_S = \frac{1}{2}\int_{V_S} \bar{E}_s^E \left(\frac{\partial U(x,z,t)}{\partial x}\right)^2 \mathrm{d}V_S. \tag{4}$$

The kinetic energy of the sensor, instead, is analogous to expression (3) obtained for the actuator, and is

$$K_S = \frac{1}{2}\rho_S \int_{V_S} \left\{ \left(\frac{\partial U(x,z,t)}{\partial t}\right)^2 + \left(\frac{\partial W(x,z,t)}{\partial t}\right)^2 \right\} \mathrm{d}V_S, \tag{5}$$

where ρ_s and $\bar{E}_s^E$ are the volume density and Young's modulus of the sensor at constant electric field. The displacements $U(x,z,t)$ and $W(x,z,t)$ are considered continuous through the cross-section and between beam-actuator and beam-sensor interfaces. The damaged area is represented with different mass density and Young's modulus while the displacements are assumed continuous through the different regions. Bernoulli's hypotheses are used and all shear effects are neglected. In this assumption the displacements are written as

$$U(x,z,t) = u(x,t) - z\frac{\partial w(x,t)}{\partial x}, \quad W(x,z,t) \equiv w(x,t), \tag{6}$$

where $u(x,t)$ and $w(x,t)$ are the longitudinal and transverse displacements of the beam's neutral axis.

The neutral axis and transverse displacements are approximated with a series expansion of sinusoidal functions coincident with the beam mode shapes

$$u(x,t)=\sum_{l=1}^{p}A_l(t)\sin\left(l\frac{\pi}{L}x\right),\quad w(x,t)=\sum_{k=1}^{q}B_k(t)\sin\left(k\frac{\pi}{L}x\right). \tag{7}$$

In this paper, 15 terms are included in each series expansion for a total of 30 terms. The displacements of Eq. (7) are substituted back into the potential and kinetic energy terms defined in Eqs. (1)–(5). By utilizing the Rayleigh–Ritz method [14] the equation of motions are recovered in terms of the coefficients $A_l(t)$ and $B_k(t)$ of the series expansion and give

$$[M]\{\ddot{X}\}+[K]\{X\}=\{F\}\Delta\varphi_a,\quad \{X\}=\left\{\begin{array}{c}A_l(t)\\B_k(t)\end{array}\right\}, \tag{8}$$

where $\{X\}$ is the generalized displacement vector, $[M]$ and $[K]$ are the generalized mass and stiffness matrices, $[F]$ is the generalized forcing term recovered from the actuator and $\Delta\varphi_a$ is the voltage input of the actuator.

The damping matrix is subsequently added to Eq. (8) by using the modal damping coefficients (ζ_i) for each mode shape obtained from test measurement

$$\zeta_i=\frac{\omega_{2i}-\omega_{1i}}{2\omega_i}. \tag{9}$$

Here, ω_i is the natural frequency and ω_{1i} and ω_{2i} are the frequencies at -3 dB from the peak values. The equivalent full viscous damping matrix ($[D]_d$) is obtained as [14]

$$[D]_d=[M][\Phi][2\omega_i\zeta_i][\Phi]^{\mathrm{T}}[M], \tag{10}$$

where $[\phi]$ is the modal matrix and $[2\omega_i\zeta_i]$ is the diagonal modal damping matrix.

The equation of motion including damping is rearranged in a linear time invariant state space form [16]

$$\{\dot{\xi}\}=[A]\{\xi\}+[\mathrm{B}]\Delta\varphi_a,\quad \{X\}=[C^*]\{\xi\},\quad \{\xi\}=\{X\vdots\dot{X}\}, \tag{11}$$

where the matrices $[A]$, $[B]$, and $[C^*]$ are assembled as follows:

$$[A]=\left[\begin{array}{cc}[O] & [I]\\ -[M]^{-1}[K] & -[M]^{-1}[D]_d\end{array}\right],\quad [\mathrm{B}]=\left[\begin{array}{c}[O]\\[F]\end{array}\right],\quad [C^*]=[[I]\quad[O]]. \tag{12}$$

From Eq. (11), the series expansion coefficients are recovered and substituted back into Eqs. (7) and (8) to obtain displacements. However, for our purpose, the voltage output from the sensor is desired. For a capacitor, the voltage output is related to the current $i(t)$ as

$$\Delta\varphi_s=\frac{1}{C_s}\int i(t)\,\mathrm{d}t \tag{13}$$

with C_s the capacitance value. The current $i(t)$ for a piezoelectric sensor is expressed in terms of strain as

$$i(t) = e_{31} \int_{Vs} \frac{\partial \varepsilon_x(x, z_S, t)}{\partial t} \, \mathrm{d}V_S, \tag{14}$$

where $\varepsilon_x(x, z_S, t)$ are the strains evaluated at the middle of the sensor thickness and the integral is extended over the sensor volume V_s. The output sensor voltage $\Delta\varphi_s$ is obtained by substituting Eq. (14) into Eq. (13). These two steps can be both included in a modified matrix $[C]$ of Eq. (11) such that the voltage $\Delta\varphi_s$ is recovered directly from the state space formulation

$$\{\dot{\xi}\} = [A]\{\xi\} + [B]\Delta\varphi_a, \quad \{\Delta\phi_s\} = [C]\{\xi\}, \quad [C] = \beta[C^*], \tag{15}$$

where β is obtained from the integration process of Eq. (14).

The input–output (I/O) relationship, or transfer function, between actuator input voltage and sensor output voltage in the frequency domain (ω) is

$$H(\omega) = \frac{\Delta\varphi_s}{\Delta\varphi_a} = [C](\mathrm{j}\omega[I] - [A])^{-1}[B]. \tag{16}$$

2.1. Power spectral density analysis

For a linear system, the output PSD, $S_{yy}(\omega)$ is defined as [15]

$$S_{yy}(\omega) = |H(\omega)|^2 S_{xx}(\omega), \tag{17}$$

where $S_{xx}(\omega)$ is the input PSD. The area under $S_{yy}(\omega)/2\pi$ equals the average output power [17]. However, in our analysis, we are interested in the relative changes between input/output energies in specific bandwidths. For historical reasons, this bandwidth-localized power is expressed by means of Root Mean Square (RMS) defined as [15]

$$\textit{Root Mean Square} = \left\{ \frac{1}{2\pi} \int_{\omega 1}^{\omega 2} |H(\omega)|^2 \, \mathrm{d}\omega \right\}^{1/2}, \tag{18}$$

where ω_1 and ω_2 are the band frequencies. In our analysis, we utilized the bandwidth between the frequencies ω_1 and ω_2 positioned at 12 dB below the ith resonance frequency of the undamaged structure. These RMS values are defined as $(RMS)_U$ and $(RMS)_D$ for undamaged and damaged structure, respectively, and can be utilized to determine whether or not the structure is damaged by the index

$$DLM = \sum_{i=1}^{N} \left| \frac{(RMS_i)_U - (RMS_i)_D}{(RMS_i)_U} \right|, \tag{19}$$

where $|(RMS_i)_U - (RMS_i)_D|$ is the absolute value of the difference between the RMS of the ith resonance modes of the undamaged and damaged structure. The ith term of the DLM index represents the influence of damage on the ith mode shape. By summing all the contributions, a

sensitive measure of damage can be developed. Therefore, this index can be utilized to assess damage in the structure, however, it is unable to distinguish stiffness variations from mass variations.

Once the structure is identified as damaged by means of the DLM index, the damage position along the structure can be estimated by introducing a *damage location function*, $DL(x)$, defined as

$$DL(x) = \sum_{i=1}^{N} \left| \frac{(RMS_i)_U - (RMS_i)_D}{(RMS_i)_U} \right| \times |\varphi_i(x)|. \tag{20}$$

Eq. (20), in addition to the quantities previously defined, includes the function $|\varphi_i(x)|$ that is the absolute value of the ith mode shape of the undamaged structure. The $DL(x)$ function can be interpreted as the sum of all the mode shapes, with each one weighted by the percentage change caused by the damage. Damage influences a particular mode shape based on its location in the structure. For example, if damage is at the anti-node of a mode shape, it strongly influences the resonant frequency. On the contrary, the resonant frequency of a mode shape is not influenced by damage positioned at one of its nodes. By summing the individual contribution at each mode shape, the $DL(x)$ function provides an indication of damage location.

3. Experimental set-up

The experimental set-up consisted of a simply supported aluminum beam with one actuator and one sensor (piezoelectrics) bonded to the structure. A photograph of the test set-up is provided in Fig. 1. The beam width and thickness were 27.5 and 2.45 mm, respectively, while its length was 771 mm. Each support was made of two sharp blades intercalated in two slots machined in the upper and lower surface of the beam. Both supports were bolted to a vibration isolation table. The piezoelectric sensor and actuator utilized were PZT 5 H with dimensions of 15 mm length, 6.7 mm

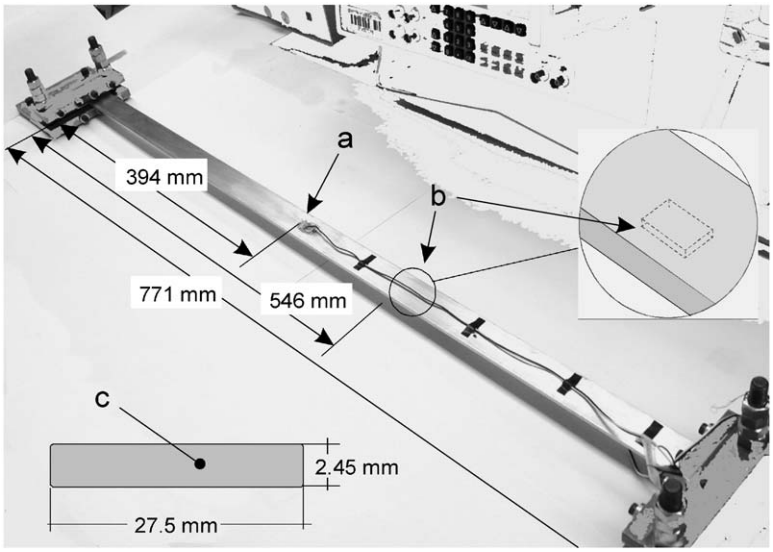

Fig. 1. Experimental test set-up of the simply supported beam: (a) actuator, (b) sensor, and (c) beam cross-section.

Table 1
Material properties

Property	Beam	Sensor/actuator
E^E (N/m^2)	68.9×10^9	42×10^9
ρ (kg/m^3)	2670	7550
ϵ^{ε} (C^2/N m^2)	—	1750
d_{31} (m/V)	—	190×10^{-12}

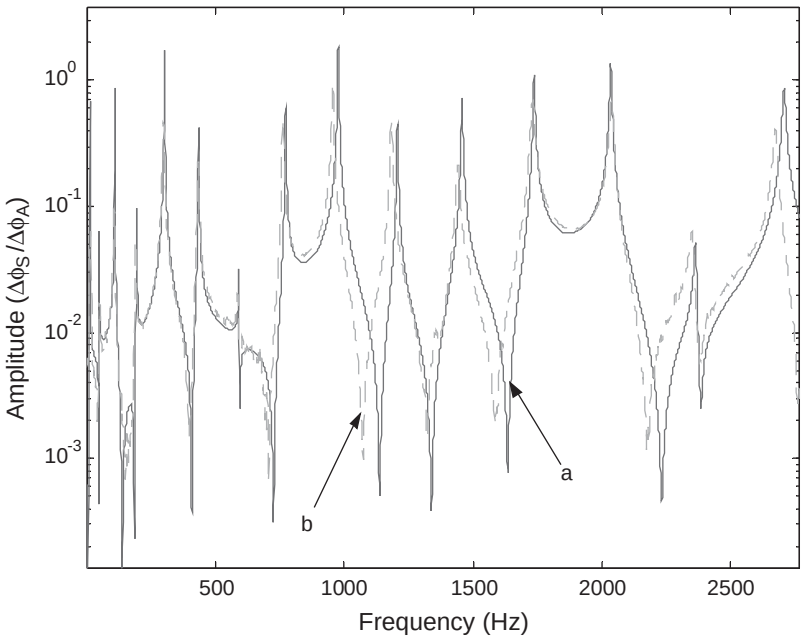

Fig. 2. Frequency response 0–2950 Hz: analytical (a) vs. experimental (b).

width and 0.6 mm thickness. The actuator was bonded on the upper surface at 394 mm from the left edge of the beam while the sensor was bonded on the lower surface at 546 mm from the left edge as shown in Fig. 1. These two locations were chosen such that all of the structure's mode shapes were excited by the actuator and sensed by the sensor without regard to the damage studied. The material properties of the beam, sensor and actuator are listed in Table 1.

The I/O frequency response was obtained using a white noise input signal produced by a Wavetek 10 MHz DDs Model 29. The white noise frequency range of 0–180 kHz was filtered to 10 kHz by a Krohn-Hite (KH) model 3382, 8 Pole Butterworth/Bessel. A Burleigh PZ 150 M 0–150 V output voltage amplifier was used to amplify the signal to the actuator. The sensor output was amplified with a Kistler type 5010B charge amplifier and subsequently filtered in the KH filter. The input and output signals were recorded with a Textronix TDS 460A, 350 MHz digitizing oscilloscope. Up to 20k points were recorded in the oscilloscope for both the input and output signals. At least 20 acquisitions were performed for each measurement and the sampling rate used was 10k sample/s. that produced a frequency resolution of 0.5 Hz. Hanning windows

Table 2
Measured natural frequencies compared with the analytically predicted ones

Natural frequency	Analytical (Hz)	Measured (Hz)	Error (%)	Natural frequency	Analytical (Hz)	Measured (Hz)	Error (%)
1	12.06	13.0	−7.7	9	976.55	954.5	2.3
2	48.16	49.0	−1.7	10	1204.15	1182.0	1.8
3	108.59	106.5	1.9	11	1458.34	1439.5	1.3
4	192.70	189.0	1.9	12	1733.61	1729.5	0.3
5	301.55	297.5	1.3	13	2035.66	2036.5	—
6	433.51	433.5	—	14	2359.52	2346.5	0.6
7	591.03	585.0	1.0	15	2708.68	2672.0	1.4
8	770.66	762.0	1.1	16	3188.1	3034.5	4.8

were used to reduce leakage effects while an overlapping technique was employed to obtain more data sets. The data were processed in the frequency domain for each window and the results were averaged. More than 50 averages were used to obtain the desired spectrum.

In Fig. 2, the spectra obtained from the analytical model and measured data are compared up to approximately 3 kHz. From the figure, it can be seen that relatively good agreement between the data and the analytical model were obtained. In Table 2 are also listed the first 16 measured frequencies compared with the model predictions. The natural frequencies from 1 to 15 are relative to bending modes and the first longitudinal frequency is measured at 3034.5 Hz. It can be seen that the error between the estimated and measured frequencies was approximately 2% or less except for the first and sixteenth frequencies. In particular, the first measured frequency differed by approximately 1 Hz from the estimated one, resulting in an error of 7.7%. Based on these results, in our model only the first 15 mode shapes were included.

4. Results

In the analytical section, we suggested that the RMS values of the PSD could be used to identify damage. A numerical example is provided to illustrate this concept. The damage was simulated by adding a 4 g mass positioned on top of the beam at its mid point. This mass was equivalent to approximately 2% of the entire mass of the structure. Although the mass does not represent actual damage, it can be positioned at multiple locations to verify the method, where actual damage cannot (i.e., one damage per test). Fig. 3 shows the resulting frequency response spectra obtained for the undamaged and damaged case in the frequency range between 1600 and 2300 Hz, thereby including the 12th and 13th flexural mode shapes. The ordinate of the plot is expressed in decibels. It is apparent that with the mass positioned at the mid-point of the beam, only the symmetric modes, such as the 13th, were affected while the antisymmetric ones, such as the 12th, were essentially unchanged. The frequency shift of the 13th mode was calculated to be 1.6% of the undamaged natural frequency. The magnitude of this value is regarded as relatively insensitive indicator of damage.

By utilizing the RMS values obtained in bandwidth near resonance, the sensitivity was increased. From Eq. (18), $(RMS)_U$ and $(RMS)_D$ values were obtained for both the undamaged

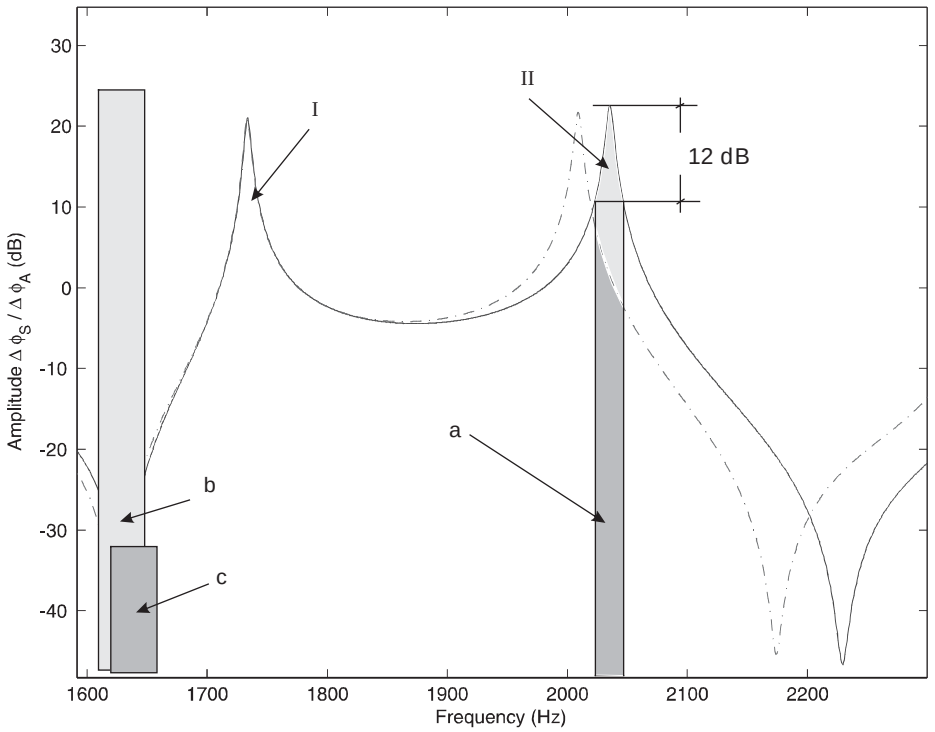

Fig. 3. Analytical data. Frequency response of undamaged and 4 g mass damage beam in the range of frequency 1600–2280 Hz: (I) 12th natural frequency, (II) 13th natural frequency, (a) 12 dB bandwidth region, (b) RMS value before damage (linear scale), (c) RMS value after damage (linear scale).

and damaged case. The percentage change of $(RMS)_U$ with respect of $(RMS)_D$ was calculated to be 84.4% for the 13th mode of Fig. 3. This is a much greater value when compared to the 1.6% frequency shift obtained previously, thus indicating that this technique is a sensitive measure of damage.

Fig. 4 shows the values of $(RMS)_U$ and $(RMS)_D$ obtained for all of the 15 mode shapes included in the analysis. Since the 13th mode presented the largest RMS change, the reported RMS values in the ordinate of the plot were normalized with respect to its value. As can be observed, large RMS variations occurred mainly in the symmetric (odd) modes such as the 5th, 9th, 11th, 13th and 15th. The DLM index (Eq. (19)) was calculated for this case and yielded $DLM = 771.9\%$. This is considerably large value that can be utilized to determine damage in the structure.

The localization of the damage was obtained with the $DL(x)$ function defined in Eq. (20). For this case, the function was calculated and plotted in Fig. 5. The ordinate of the plot indicates the $DL(x)$ value normalized with respect to its peak value while the abscissa represents the length of the beam in meters. It is immediately apparent that the maximum of the $DL(x)$ function coincides with the location of the 4 g mass. The difference between this dominant peak and the mean value was calculated to be approximately 35%.

While the previous numerical example uses a mass positioned at the mid-point of the structure, the following one incorporates a smaller mass positioned at an off center location. The analytical

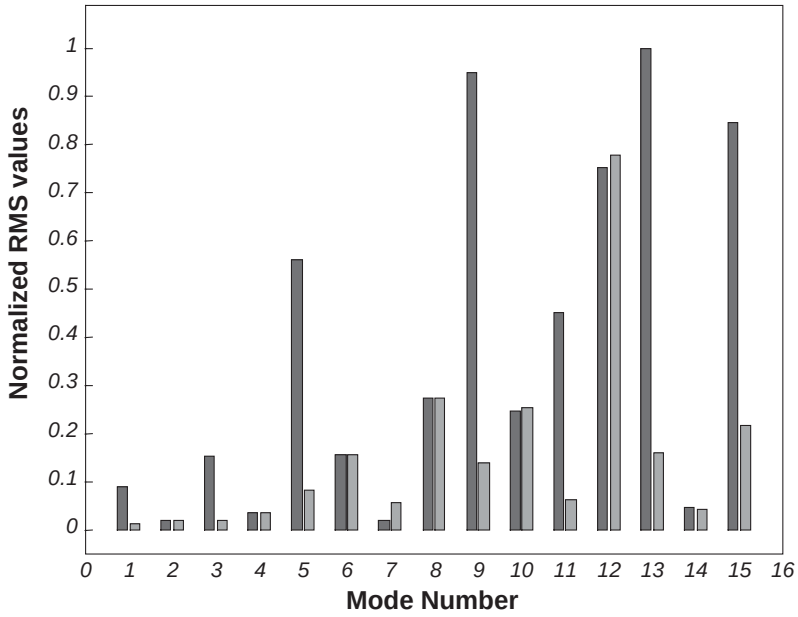

Fig. 4. Analytical data. Normalized RMS values for undamaged and 4 g damaged structure for the 15 flexural mode shapes. (I) Black columns are undamaged structure values, (II) gray columns are damaged structure values.

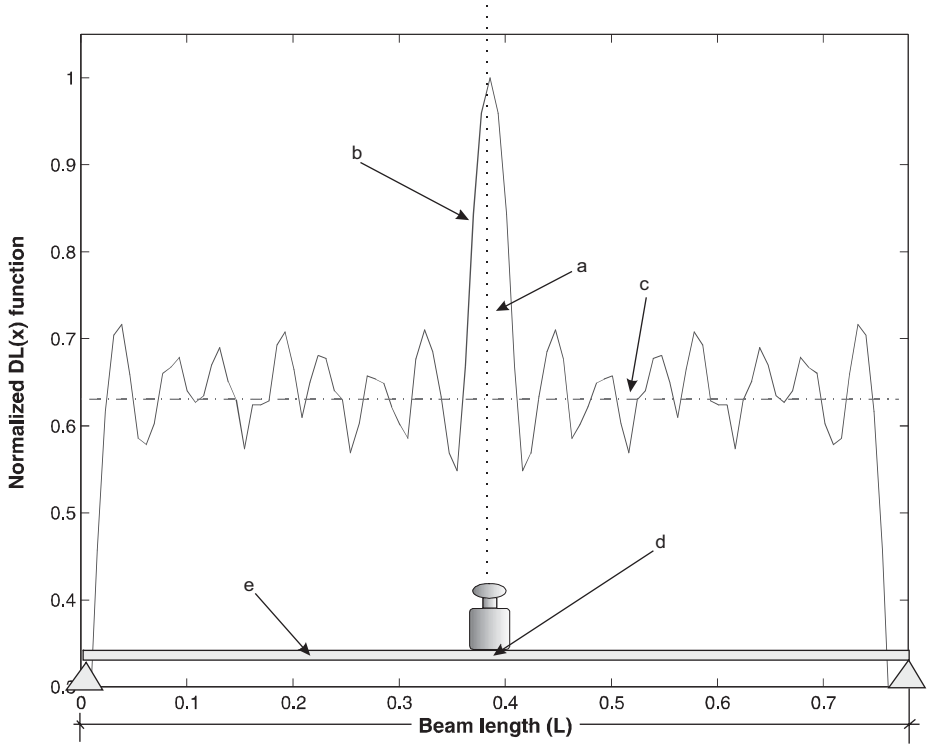

Fig. 5. Analytical data. Normalized damage location function, $DL(x)$, calculated for 4 g mass damage. (a) Symmetric axis, (b) $DL(x)$ function, (c) $DL(x)$ mean value, (d) mass position, $x = L/2$, (e) simply supported beam scheme.

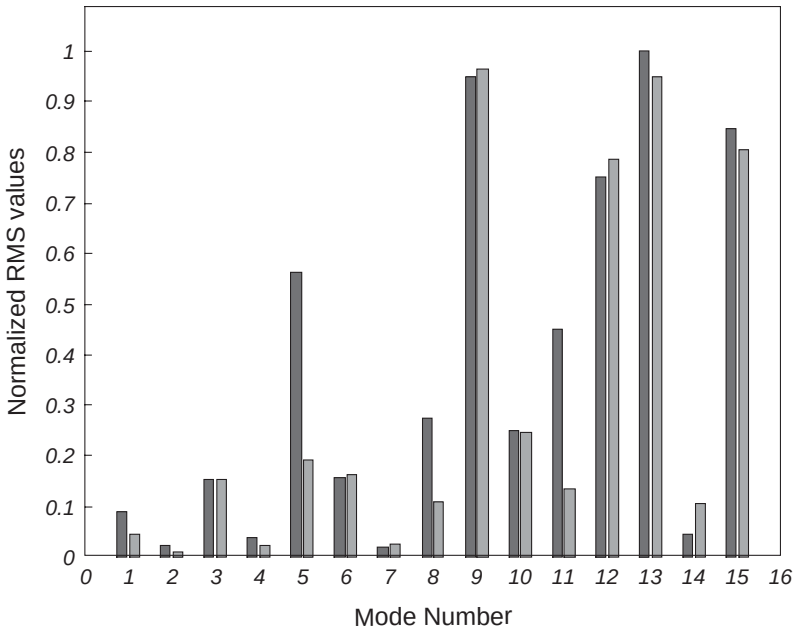

Fig. 6. Analytical data. Normalized RMS values of all the 15 mode shapes for undamaged and 2 g mass damage positioned at $x = 244$ mm. (I) black columns are undamaged structure values, (II) gray columns are damaged structure values.

method was evaluated on a beam containing a 2 g mass positioned at 244 mm from the left support. The mass was equivalent to approximately 1% of the entire structure mass. In Fig. 6, the $(RMS)_U$ and $(RMS)_D$ values obtained from our computational analysis are plotted for all of the 15 mode shapes considered. The reported RMS values in the ordinate were normalized with respect to the $(RMS)_U$ value of the 13th mode which had the greatest value. The most prominent percent changes of $(RMS)_U$ with respect to $(RMS)_D$ were observed for the 5th, 8th and 11th modes and were calculated to be 65.7% and 70.7% and 68.3%, respectively. The DLM index was $DLM = 517.7\%$ which, is less than the DLM index obtained for the case of 4 g mass.

In order to locate the damage, the damage location function $DL(x)$ was calculated for this case and is plotted in Fig. 7. As usual, the $DL(x)$ function was normalized with respect to its peak value and plotted vs. the entire beam length. It can be seen that this scenario produced two dominant peaks symmetric with respect to the mid-point of the structure and one of which was coincident with the mass position ($x = 244$ mm). The symmetry occurred because the two locations produced equal changes to the structure's mode shapes. The percent difference between the dominant peak and the mean value was considerably high and was calculated to be approximately 30%.

Experimental data for the beam containing a 2 g mass positioned at 244 mm from the left support were also generated and the RMS changes obtained for all the 15 mode shapes are shown in Fig. 8. The reported values in the ordinate are normalized with respect to the $(RMS)_U$ value of the 12th mode which produced the largest value. From the figure, the most prominent percent changes of $(RMS)_U$ with respect to $(RMS)_D$ were observed for the 8th and 11th modes and were calculated to be 41.1% and 35.7%, respectively. By comparing the analytical data reported in

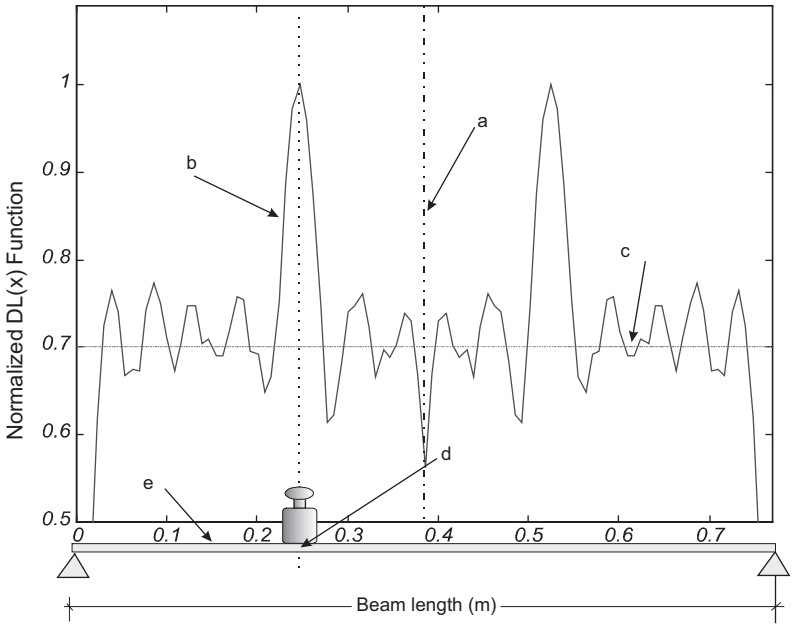

Fig. 7. Analytical data. Normalized damage location function, $DL(x)$, for 2 g mass. (a) Symmetric axis, (b) $DL(x)$ function, (c) $DL(x)$ mean value, (d) mass position, $x = 244$ mm, (e) simply supported beam scheme.

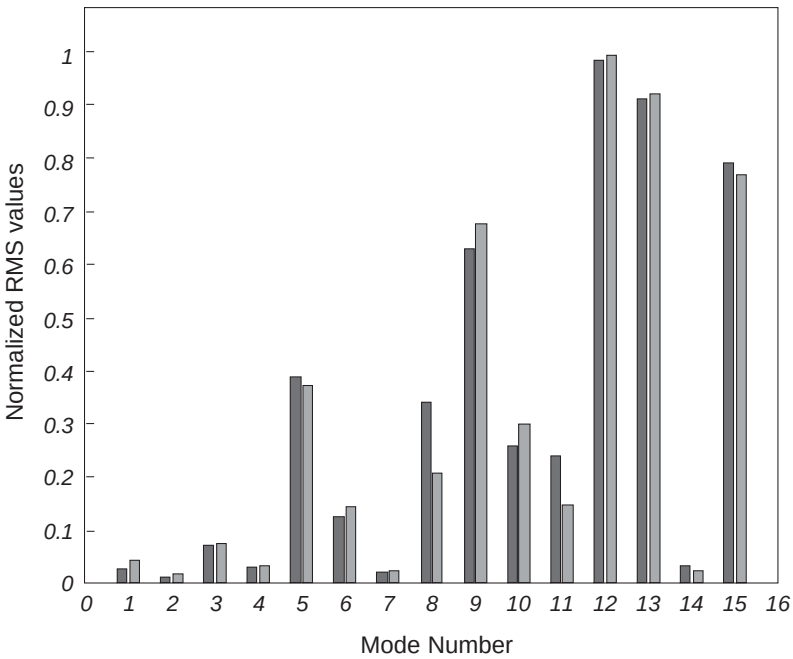

Fig. 8. Experimental data. Normalized RMS values of all the 15 mode shapes for undamaged and 2 g mass damage positioned at $x = 244$ mm. (I) black columns are undamaged structure values, (II) gray columns are damaged structure values.

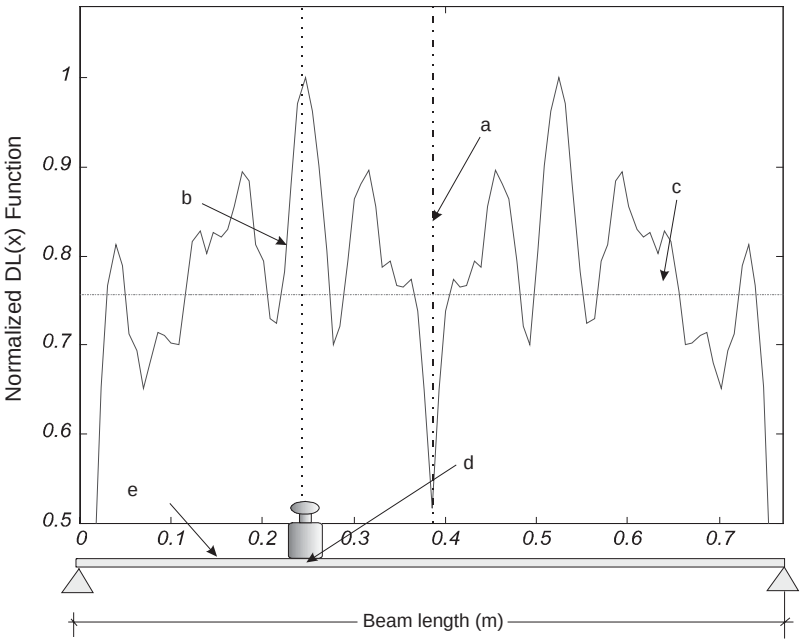

Fig. 9. Experimental data. Normalized damage location function, $DL(x)$, for 2 g mass: (a) symmetric axis, (b) $DL(x)$ function, (c) $DL(x)$ mean value, (d) mass position, $x = 244$ mm, (e) simply supported beam scheme.

Fig. 6, with the experimental data reported in Fig. 8, one can see that the RMS changes of the 8th and 11th modes were predicted by the model and verified experimentally, while the RMS change predicted for the 5th mode was not verified by experimental data. The DLM index calculated from measured data yielded $DLM = 416.4\%$ while numerical simulation predicted $DLM = 517.7\%$. These differences indicated a decrease in sensitivity of our experimental data when compared with numerical analysis.

The normalized damage location function $DL(x)$ from experimental data using the 2 g mass, was also calculated and is presented in Fig. 9. From the figure, it can be seen that, analogously to the numerical simulation, the $DL(x)$ function produced two identical symmetric peaks, one of which was coincident with the mass position. The percent difference between the prominent peak and the mean value is approximately 25%, which compares well with the analytical value of 30%. However, in Fig. 9, the next dominant peak is approximately 10% below the prominent peak and although this margin is well above the experimental error, the 2 g mass could be regarded as approaching the threshold level of identifiable damage.

While the previous examples relied on adding mass to simulate damage, we also investigated the effect of a saw cut of 3.5 mm deep and 1 mm wide made in one side of the beam at 239 mm from the left support. This cut represented 12.7% of the beam width. It is known that these kinds of cuts produce insignificant variation in resonant frequencies of the structure (see Ref. [8]). In the current case, the frequency response remained substantially unchanged as seen from Fig. 10, which illustrates the transfer functions obtained experimentally between 250 and 500 Hz for the damaged and undamaged beam. This range of frequency included the 5th and 6th resonant frequencies. From the figure, one can see that the two natural frequencies did not shift

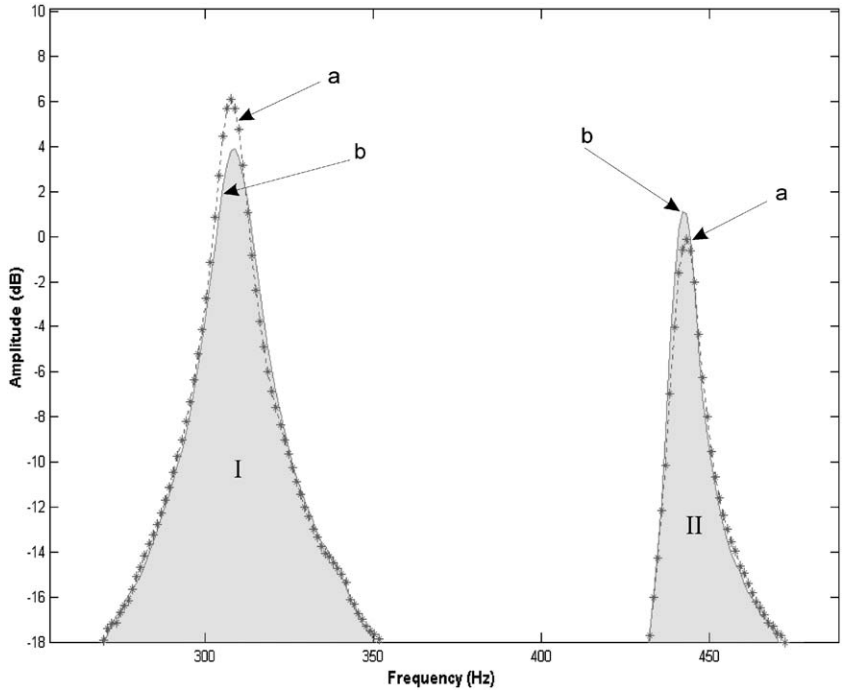

Fig. 10. Experimental data. Frequency response of undamaged beam and 3.5×1 mm saw cut damage made at $x = 239$ mm. (I) 5th natural frequency, (II) 6th natural frequency, (a) damaged structure response, (b) undamaged structure response.

substantially and that the only significant changes were observed in the peak amplitudes. The RMS difference between undamaged and damaged structure for the 5th and 6th modes shown, were calculated to be 15.1% and 10.9%, respectively. We highlight the fact that, for this scenario, frequency shift analysis is substantially less sensitive than the RMS analysis proposed. The DLM index calculated for all of the 15 natural frequencies for this scenario yielded $DLM = 172.41\%$.

The damage location function $DL(x)$ was also obtained from the experimental data and is plotted in Fig. 11. As usual, the $DL(x)$ function was normalized with respect to its maximum value. As can be seen, one of the two symmetric $DL(x)$ maxima coincides with the position of the saw cut, thereby locating the damage. However, from the figure it can be seen that the other prominent peaks have amplitudes that are comparable with the amplitude of the peak locating the cut. Thus, we considered the 3.5 mm saw cut as the threshold value of damage detection for the proposed method.

5. Conclusion

A method for identification and localization of structural damage is implemented analytically and experimentally for a simply supported beam. The method focuses on bandwidth-localized energy that is most sensitive to damage. The sensitivity increases considerably when compared

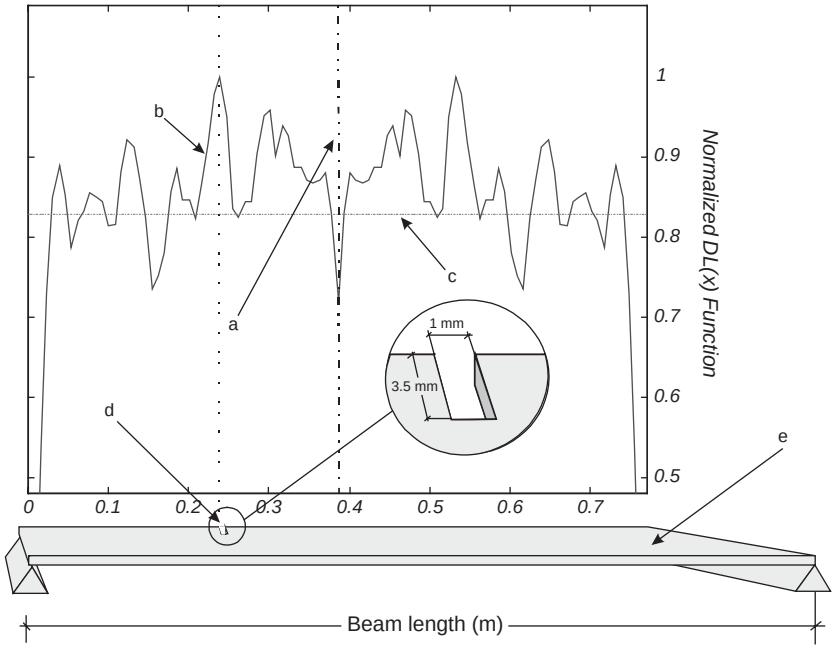

Fig. 11. Experimental data. Normalized damage location function, $DL(x)$, for 3.5×1 mm saw cut: (a) symmetric axis, (b) $DL(x)$ function, (c) $DL(x)$ mean value, (d) saw cut position, $x = 239$ mm, (e) simply supported beam scheme.

with frequency shifts. In order to simulate damage, two small masses, 4 and 2 g, representing 2% and 1%, respectively, of the entire structural mass, are added to the structure in two distinct cases and localized. In particular, the 2 g mass is localized by using experimental data confirming the analytical prediction. In addition to mass-type damage, a saw cut damage created on one edge of the structure is analyzed by using experimental data. Although this scenario was revealed to be particularly challenging the saw cut was detected and localized.

Acknowledgements

The authors would gracefully acknowledge NASA Dryden Flight Research Center for supporting this work with grant NCC4-153: Pr. 32.

References

[1] P. Cawley, R.D. Adams, The location of defects in structures from measurements of natural frequencies, *Journal of Strain Analysis* 14 (2) (1979) 49–57.

[2] D. Armon, Y. Ben-Haim, S. Braun, Crack detection in beams by rank-ordering of eigenfrequency shifts, *Mechanical Systems Signal Processing* 8 (1) (1994) 81–91.

[3] S.W. Doebling, C.R. Farrar, M.B. Prime, Damage identification and health monitoring of structural and mechanical systems from changes in their vibration characteristics: a literature review, Los Alamos National Laboratory, Los Alamos, NM, 1996.
[4] O.S. Salawu, Detection of structural damage through changes in frequency: a review, *Engineering Structures* 19 (9) (1997) 718–723.
[5] Y. Narkis, Identification of crack location in vibrating simply supported beams, *Journal of Sound and Vibration* 172 (4) (1994) 549–558.
[6] A. Morassi, Identification of a crack in a rod based on changes in a pair of natural frequencies, *Journal of Sound and Vibration* 242 (4) (2001) 577–596.
[7] A. Morassi, M. Dilena, On point mass identification in rod and beams from minimal frequency measurements, *Inverse Problems in Engineering* 10 (3) (2002) 183–201.
[8] C.R. Farrar, W.E. Baker, T.M. Bell, K.M. Cone, T.W. Darling, T.A. Duffey, A. Eklund, A. Migliori, Dynamic characterization and damage detection in the I-40 bridge over the Rio Grande, Los Alamos National Laboratory Report LA-12767-MS, 1994.
[9] W.M. West, Illustration of the use of modal assurance criterion to detect structural changes in an orbiter test specimen, *Proceedings of the Air Force Conference on Aircraft Structural Integrity*, 1984, pp. 1–6.
[10] J.-H. Kim, H.-S. Jeon, C.-W. Lee, Application of the modal assurance criteria for detecting and locating structural faults, *Proceedings of the 10th International Modal Analysis Conference*, San Diego, CA, 1992, pp. 536–540.
[11] A.K. Pandey, M. Biswas, M.M. Samman, Damage detection from changes in curvature mode shapes, *Journal of Sound and Vibration* 145 (2) (1991) 321–332.
[12] N. Stubbs, J.-T. Kim, K. Topole, An efficient and robust algorithm for damage localization in offshore platforms, *Proceedings of the ASCE 10th Structures Congress*, 1992, pp. 543–546.
[13] S. Park, N. Stubbs, R. Bolton, S. Choi, C. Sikorsky, Field verification of the damage index method in a concrete box-girder bridge via visual inspection, *Computer-Aided Civil and Infrastructure Engineering* 16 (1) (2001) 58–70.
[14] P.L. Gatti, V. Ferrari, *Applied Structural and Mechanical Vibrations—Theory, Methods and Measuring Instrumentation*, E. &FN Spon, London, 1999.
[15] V.Z. Parton, B.A. Kudryavtsev, *Electromagnetoelasticity*, Gordon and Breach Science Publisher, New York, 1988.
[16] C.-T. Chen, *Linear System Theory and Design*, Oxford University Press, New York, 1984.
[17] A. Papoulis, *Probability Random, Variables and Stochastic Processes*, McGraw-Hill Inc., New York, 1965.